SUPPLEMENTARY MATERIALS

1. Appendix A: Formal derivation

We outline how the minimal aging model arises from coarse–graining the high-dimensional dynamics of molecular and physiological variables.

a. Onsager formalism. Let $\mathbf{x} = (x_1, \ldots, x_N)$ denote the organismal state. Near an equilibrium point $\mathbf{x}_*$ we define deviations $\mathbf{z} = \mathbf{x} - \mathbf{x}_*$, which follow the Onsager form

$$\dot{z}_\alpha = -\sum_\beta L_{\alpha\beta} \frac{\partial U(\mathbf{z})}{\partial z_\beta} + J_\alpha + f_\alpha, \tag{2}$$

where $L_{\alpha\beta}$ is the Onsager matrix, U an effective potential, J_α persistent external stresses, and f_α Gaussian white noise with covariance $\langle f_\alpha(t) f_\beta(t+\tau)\rangle = 2D_{\alpha\beta}\delta(\tau)$.

b. Hessian expansion and normal modes. Expanding U to quadratic order,

$$\frac{\partial U}{\partial z_\alpha} \simeq \sum_\beta H_{\alpha\beta} z_\beta,$$

yields linear dynamics

$$\dot{\mathbf{z}} = -K\mathbf{z} + \mathbf{J} + \mathbf{f} + \mathcal{O}(\mathbf{z}^2), \tag{3}$$

where $K = LH$ is the stability matrix. Its eigenvectors define normal modes and its eigenvalues $\{\varepsilon_\alpha\}$ define corresponding relaxation rates. All modes except one have strictly positive real parts and relax rapidly.

c. Why linear coupling cannot generate aging. The most general linear system

$$\dot{z}_\alpha = -\sum_\beta K_{\alpha\beta} z_\beta + f_\alpha(t)$$

can always be diagonalized. In this basis,

$$\dot{z}_\alpha = -\tilde{\varepsilon}_\alpha z_\alpha + f_\alpha(t),$$

and the eigenvalues $\tilde{\varepsilon}_\alpha$ are fixed. Thus purely linear coupling cannot produce a progressive, age-dependent softening of the critical mode. Aging must arise from *nonlinear* interactions and slow deformation of the underlying landscape.

d. Nonlinear couplings. Retaining weak nonlinearities, the normal modes satisfy

$$\dot{z}_0 = -\varepsilon_0 z_0 + g_{000} z_0^2 + \sum_a g_{0a0} z_0 z_a + \sum_{ab} g_{0ab} z_a z_b + J_0 + f_0, \tag{4}$$

$$\dot{z}_a = -E_a z_a + g_{a00} z_0^2 + 2\sum_{b\neq a} g_{a0b} z_0 z_b + \sum_{bc} g_{abc} z_b z_c + J_a + f_a, \tag{5}$$

where $E_a = \varepsilon_a > 0$ are the fast relaxation rates and $g_{\alpha\beta\gamma}$ are "bare" nonlinear couplings (their values on short time scales).

e. Enslavement of fast modes. Because $|\varepsilon_0| \ll E_a$, the fast modes relax rapidly to quasi-steady values determined by the instantaneous value of z_0. To lowest order in the nonlinear couplings,

$$z_a(t) \simeq \Delta z_a + \frac{g_{a00}}{E_a} z_0^2(t) + \frac{J_a}{E_a}, \tag{6}$$

where Δz_a is the equilibrium position of the ath fast mode at $z_0 = 0$. Substituting Eq. (6) into Eq. (4) and retaining terms up to $\mathcal{O}(g)$ yields the coarse–grained equation

$$\dot{z}_0 = -\varepsilon_0^{\text{eff}} z_0 + g^{\text{eff}} z_0^2 + J_0^{\text{eff}} + f_0^{\text{eff}}, \tag{7}$$

with renormalized coefficients

$$\varepsilon_0^{\text{eff}} = \varepsilon_0 - \sum_a g_{0a0} \Delta z_a, \tag{8}$$

$$g^{\text{eff}} = g_{000} + \sum_a g_{0a0} \frac{g_{a00}}{E_a}, \tag{9}$$

$$J_0^{\text{eff}} = J_0 + \sum_{ab} g_{0ab} \Delta z_a \Delta z_b. \tag{10}$$

These renormalizations arise from the polarization of the fast modes slaved to z_0. Crucially, no time dependence appears unless the Δz_a themselves evolve.

f. Irreversible microscopic events and the emergence of $Z(t)$. Rare, effectively irreversible microscopic events—mutations, epimutations, crosslinks, chromatin transitions, and other configurational changes—deform the fast-mode landscape. Each such event produces a small shift

$$\Delta z_a \;\to\; \Delta z_a + \delta\Delta z_a.$$

Because these shifts are individually tiny but numerous, they accumulate into a slow entropic damage variable $Z(t)$:

$$Z(t) = \sum_{\text{events}} 1, \qquad \dot{Z} = \gamma.$$

To leading order,

$$Z(t) \simeq \gamma t.$$

As Δz_a become functions of Z, the renormalized coefficients in Eq. (7) acquire Z-dependence. In particular,

$$\varepsilon_0(Z) = \varepsilon_0 - \sum_a g_{0a0}\Delta z_a(Z) \;\approx\; \varepsilon_0 - \beta' Z, \tag{11}$$

and similarly the drift coefficient becomes

$$J_0(Z) = J_0 - \beta_Z Z. \tag{12}$$

Both β' and β_Z encode how sensitive the slow-mode drift and stability are to accumulated entropic damage.

g. Final coarse–grained dynamics. Collecting all terms depending on Z, we obtain the minimal long-timescale dynamics:

$$\begin{cases} \dot{z}_0 = \beta Z - \varepsilon_0(Z)\, z_0 + g\, z_0^2 + J_0 + f_0, \\ \dot{Z} = \gamma. \end{cases} \tag{13}$$

Here

$$\varepsilon_0(Z) = \varepsilon_0 - \beta' Z, \qquad \beta Z \equiv -\big(J_0(Z) - J_0\big),$$

and f_0 is an effective Gaussian noise with variance D_0.

Equation (13) shows explicitly how: (i) fast modes enslaved to z_0 feed back through their polarized values; (ii) irreversible microscopic events produce the cumulative entropic variable Z; and (iii) the slow evolution of $\Delta z_a(Z)$ induces a progressive, approximately linear renormalization of the effective drift and stability of the slow resilience mode z_0. This mechanism generates the universal dynamical signatures of aging discussed in the main text.

2. Appendix B: Extended phenomenology

Mathematical details for Class I/II animals, full survival derivations, mouse and worm datasets.

3. Class I: "unstable" animals

In the unstable regime, the critical mode z_0 begins life with a negative intrinsic recovery rate, $\varepsilon_0(Z=0) < 0$. This represents the extreme case where instability is present from the outset: physiological fluctuations are unconstrained, and resilience is absent from birth. In such systems, the slow accumulation of generalized damage Z plays only a secondary role, especially when the nonlinear couplings in Eqs. 1 are small. Mortality trajectories are therefore governed primarily by the intrinsic instability of z_0. This regime, analyzed in detail by [1], follows a characteristic sequence of phases.

Early in life, stochastic fluctuations dominate, and the variance of z_0 grows until it reaches $z_{\min}^2 \sim D_0/\alpha$, where $\alpha = |\varepsilon_0|$. Beyond this point, deterministic forces prevail, the effects of fluctuations may be neglected, and the mode variable grows exponentially along with its variance:

$$\text{mean}(z_0) \sim z_{\min}\, \exp(\alpha t), \quad \text{var}(z_0) \approx \frac{D_0}{2\alpha} \exp(2\alpha t).$$

Eventually, the system crosses a nonlinear threshold at $z_{\max} = \alpha/g$, beyond which z_0 diverges hyperbolically—a state incompatible with survival.

The average lifespan is therefore set by the threshold-crossing time

$$t_{\rm ls} = \alpha^{-1} \ln \xi, \quad \xi = \frac{z_{\max}}{z_{\min}}.$$

Because lifespan in unstable species is typically several times longer than the mortality-rate doubling time (MRDT $\sim \alpha^{-1}$), this implies $t_{\rm ls} \gg \alpha^{-1}$, hence $\xi \gg 1$. Since $\xi \sim 1/g$, the nonlinearity g must be effectively small, explaining why most of life is spent in the exponential phase.

This prediction is supported by DNA methylation (DNAm) data in mice, which reveal two major signatures: (i) a linear component linked to damage accumulation (Z) and (ii) an exponential trend reflecting intrinsic instability along z_0 [2]. A similar exponential component was recovered from longitudinal blood cell counts in the Mouse Phenome Database [3] using model-based fits of Eqs. (1) in [4], with doubling times matching empirical MRDTs - precisely as predicted by the model.

As derived previously in [1], survival probability takes the form $S(t) = \mathrm{Erf}(\xi e^{-\alpha t})$. Around the mean lifespan $t_{\rm ls}$, mortality follows an approximate Gompertz law:

$$M(t) \approx 0.6\,\alpha\, \exp[\alpha(t - t_{\rm ls})],$$

so the observed mortality doubling rate near midlife equals $\alpha = |\varepsilon_0|$. This implies that hazard curves around the average lifespan can be used to estimate α directly.

Because mortality depends strongly on α but only logarithmically on noise and nonlinearity through ξ, survival curves across conditions collapse under age rescaling by mean lifespan. This property has been validated experimentally in *C. elegans* [5].

The model also predicts systematic deviations from a pure Gompertz trajectory: shortly beyond the average lifespan, mortality acceleration slows and ultimately plateaus at a level close to the inverse MRDT, $M(t \to \infty) = \alpha$. Such deceleration and late-life plateaus have been observed in ultra-large cohorts and across multiple species [1, 6], including *C. elegans*, where the plateau matches the Gompertz slope measured earlier in life across strains with tenfold lifespan differences [7], and in mice from ITP studies, as analyzed in [4].

4. Class II: "stable" animals

Unlike unstable species, "stable" animals begin life with positive intrinsic recovery rates, $\varepsilon_0(0) > 0$. Their physiology can rebound from perturbations, maintaining a resilient equilibrium state. Early in life, fluctuations of the critical mode z_0 are suppressed by strong restoring forces, and aging manifests primarily through the slow, linear accumulation of damage Z, which steadily erodes stability.

When $Z = 0$ and external stress is absent ($J_0 = 0$), the free-energy landscape contains two fixed points: a stable minimum at $z_0 = 0$ and an unstable maximum at $z_0 = \varepsilon_0/g$, which defines the protective barrier $U_{\max} = \varepsilon_0^3/(6g^2)$ (Fig. S1). As damage accumulates, $\varepsilon_0(Z)$ declines approximately linearly, shrinking the distance between the fixed points and lowering the barrier. At the critical damage level $Z_{\max} = \gamma t_{\max}$, the recovery rate vanishes, $\varepsilon_0(Z_{\max}) = 0$, and the barrier collapses in a saddle–node bifurcation. This transition defines the species-specific maximum lifespan,

$$t_{\max} = \frac{\varepsilon_0}{\beta' \gamma},$$

set by the initial stability margin, the coupling to damage, and the accumulation rate.

As $t \to t_{\max}$, both the mean and variance of z_0 diverge hyperbolically,

$$\mathrm{mean}(z_0),\ \mathrm{var}(z_0) \sim \frac{1}{t_{\max} - t}.$$

Persistent perturbations (J_0) shift the mean but do not alter the variance, which is driven exclusively by $Z \propto t$.

These predictions align closely with empirical data. Principal component analyses of mammalian DNA methylation consistently reveal (i) a linear component reflecting steady damage accumulation and (ii) a hyperbolically diverging component projecting to the species' maximum lifespan (about 120 years in humans [8, 9]). Similar divergence has been documented in mortality-linked biomarkers including blood cell counts, physical activity, and composite metrics such as PhenoAge [10].

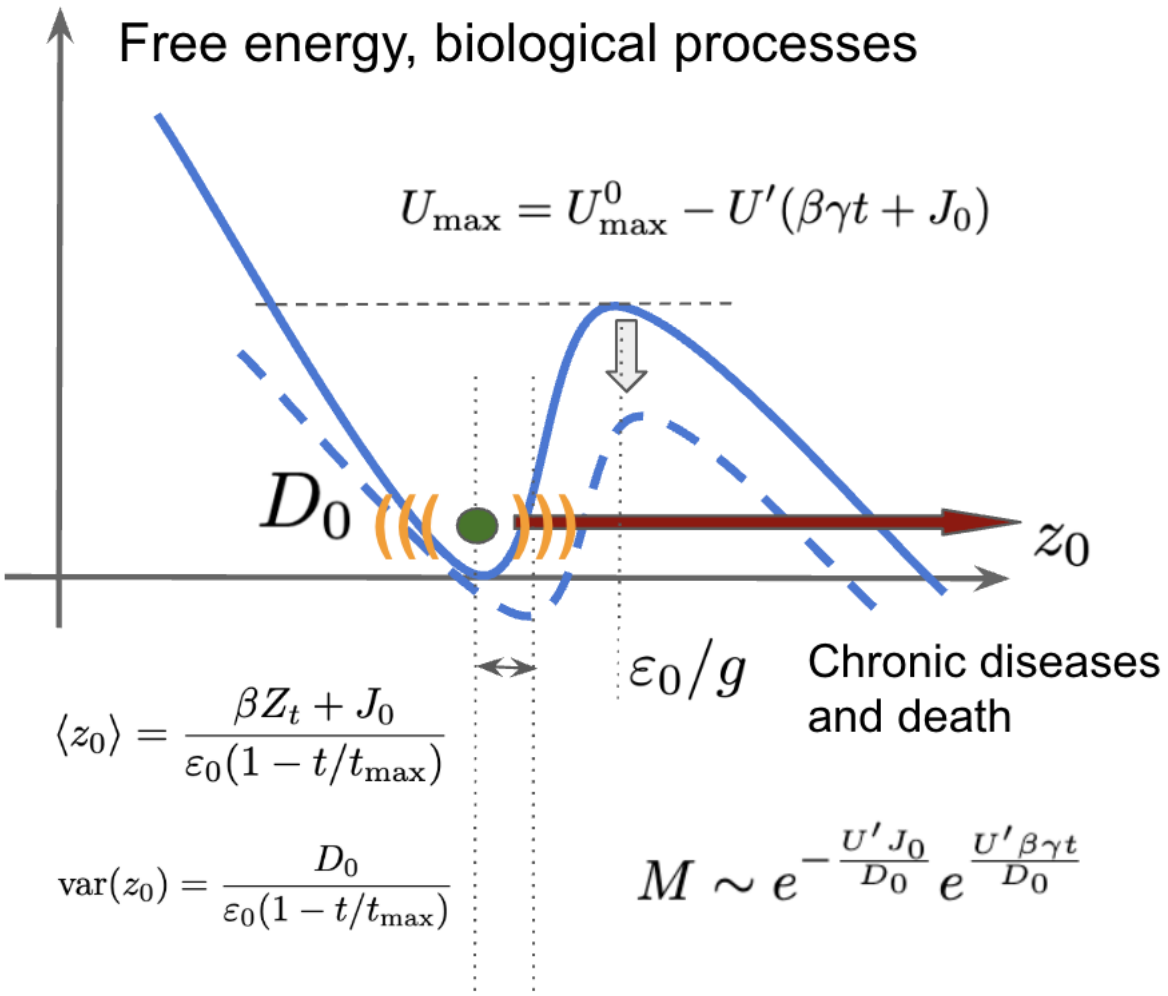

FIG. S1. Stress and damage cumulatively erode the basin of attraction for the critical mode fluctuations. This erosion drives divergence in both the mean and variance of the critical mode while exponentially increasing the probability of escape transitions leading to death. The mechanism provides a natural explanation for the Gompertz mortality law, with the Gompertz exponent (inverse mortality rate doubling time, MRDT) proportional to the damage accumulation rate and inversely proportional to the magnitude of regulatory noise.

Death, however, typically occurs earlier, when stochastic fluctuations push z_0 beyond the unstable point. Drawing on a foundational result from statistical mechanics, Kramers' theory [11], mortality risk can be expressed as the probability of crossing an energy barrier that separates stable from unstable states:

$$M(t) \sim \exp\left(-\frac{U_{\max}(Z, J_0)}{D_0}\right).$$

In the context of aging, this corresponds to the likelihood that resilience is lost and the organism transitions irreversibly from a functional to a failing state. Before $t_{\max}$, the barrier height declines approximately linearly with Z, $U_{\max} \approx U_0 - U'Z$, leading to exponential growth of mortality with age. This mechanism explains the ubiquity of the Gompertz law despite the fact that most types of molecular damage only accumulate linearly with age [12–14].

Note, that the Gompertz slope,

$$\alpha_G = \frac{U'\gamma}{D_0},$$

is directly proportional to the damage accrual rate and inversely proportional to noise strength.

A key implication is that the gap between average and maximum lifespan is determined by D_0. In the noiseless limit ($D_0 \to 0$), barrier crossing would not occur until $t_{\max}$, eliminating the gap between average and maximum lifespan. In reality, stochastic fluctuations ensure that death typically occurs before $t_{\max}$, is reached, producing the observed distribution of lifespans. Empirical estimates of D_0 from DNA methylation variance across mammals [9] confirm these model predictions. Thus, in stable animals, the combination of linear damage accumulation and stochastic barrier crossing explains both Gompertzian mortality and the separation of mean and maximum lifespan.

5. Dynamic markers of aging and resilience

The model makes strong predictions for longitudinal data. The distinction between stable ($\varepsilon_0 > 0$) and unstable ($\varepsilon_0 < 0$) regimes can be revealed through the temporal autocorrelation function (TAC) of the critical mode z_0:

$$C(\tau) = \langle z_0(t+\tau)\, z_0(t) \rangle_t,$$

where $\langle \cdot \rangle_t$ denotes averaging first along individual trajectories and then across the cohort. Intuitively, the TAC measures how similar an organism's present state remains to its past self over time. TAC analysis indicates not only whether a system is stable or unstable, but also quantifies the progressive decline of resilience as species approach the stability boundary.

In the stable regime, the TAC decays exponentially,

$$C(\tau) = \frac{D_0}{2\varepsilon_0}\, e^{-\varepsilon_0 \tau},$$

allowing ε_0 to be estimated directly from longitudinal data. Its inverse, ε_0^{-1}, has the natural interpretation of a recovery time and thus provides a quantitative measure of resilience (see Appendix B for derivation).

Because $\varepsilon_0(Z)$ decreases with accumulated damage, longitudinal analyses of human cohorts should reveal a progressive slowing of autocorrelation rates with age—a hallmark of impending failure in the form of critical slowing down.

This pattern is indeed observed: autocorrelation times derived from complete blood counts and daily physical activity increase approximately linearly with age and extrapolate to zero around $t_{\max} \approx 120$ years [10]. This behavior is consistent with Eq. 1, in which variance diverges as resilience vanishes at the maximum lifespan. These data also suggest that D_0 remains roughly age-independent, since the observed increase in variance with age is fully explained by declining resilience without requiring an increase in stochastic fluctuations.

By contrast, in unstable species the TAC should show no age-related decay. Experimentally, In [4] we analyzed the Mouse Phenome Database [3] and found TACs essentially flat over 14–28 week intervals—far exceeding the ∼4-week decay observed in humans. This absence of decay reflects the lack of a restoring force in the unstable regime and highlights the sharp difference in resilience dynamics across species.

Diverging patterns in TAC can therefore serve as dynamic markers of health and vulnerability. In [15], we showed that individuals with TAC values exceeding three months, indicative of lost dynamical stability, could be identified from longitudinal physical activity data. Importantly, their prevalence doubled approximately every seven years, consistent with Kramers' barrier-crossing theory and the human mortality-rate doubling time of ∼8 years.

The same framework also yields testable predictions for interventions. In unstable animals, perturbations of z_0 produce persistent effects detectable in short-term studies, whereas in stable species TAC decays rapidly, so intervention effects fade once treatment ends. Smoking provides a familiar example: it elevates aging biomarkers, including epigenetic clocks, yet these changes reverse quickly after cessation [10, 15, 16]. More broadly, this difference in response to perturbations explains why short-lived models may overestimate the persistence of anti-aging interventions in humans.

[1] D. Podolskiy, I. Molodtcov, A. Zenin, V. Kogan, L. I. Menshikov, V. N. Gladyshev, R. J. S. Reis, and P. O. Fedichev, arXiv preprint arXiv:1502.04307 (2015).

[2] K. Perevoshchikova and P. O. Fedichev, bioRxiv , 2024 (2024).

[3] M. A. Bogue, V. M. Philip, D. O. Walton, S. C. Grubb, M. H. Dunn, G. Kolishovski, J. Emerson, G. Mukherjee, T. Stearns, H. He, V. Sinha, B. Kadakkuzha, G. Kunde-Ramamoorthy, and E. J. Chesler, Nucleic Acids Research **48**, D716 (2020), rRID:SCR_003212.

[4] K. Avchaciov, M. P. Antoch, E. L. Andrianova, A. E. Tarkhov, L. I. Menshikov, O. Burmistrova, A. V. Gudkov, and P. O. Fedichev, Nature Communications **13**, 6529 (2022).
[5] N. Stroustrup, W. E. Anthony, Z. M. Nash, V. Gowda, A. Gomez, I. F. López-Moyado, J. Apfeld, and W. Fontana, Nature **530**, 103 (2016).
[6] J. W. Vaupel, J. R. Carey, K. Christensen, *et al.*, Science **280**, 855 (1998).
[7] A. E. Tarkhov, R. Alla, S. Ayyadevara, M. Pyatnitskiy, L. I. Menshikov, R. J. Shmookler Reis, and P. O. Fedichev, Scientific Reports **9**, 7368 (2019).
[8] A. E. Tarkhov, K. A. Denisov, and P. O. Fedichev, AgingBio **2**, e20240031 (2024).
[9] K. A. Denisov, J. Gruber, and P. O. Fedichev, bioRxiv , 2024 (2024).
[10] T. V. Pyrkov, K. Avchaciov, A. E. Tarkhov, L. I. Menshikov, A. V. Gudkov, and P. O. Fedichev, Nature communications **12**, 2765 (2021).
[11] J. P. Sethna, *Entropy, Order Parameters, and Complexity* (Oxford University Press, Oxford, UK, 2006).
[12] J. Gruber, L. F. Ng, S. Fong, Y. T. Wong, S. A. Koh, C.-B. Chen, G. Shui, W. F. Cheong, S. Schaffer, M. R. Wenk, *et al.*, PloS one **6**, e19444 (2011).
[13] R. S. Sohal and W. C. Orr, Free Radical Biology and Medicine **52**, 539 (2012).
[14] M. L. Hamilton, H. Van Remmen, J. A. Drake, H. Yang, Z. M. Guo, K. Kewitt, C. A. Walter, and A. Richardson, Proceedings of the National Academy of Sciences **98**, 10469 (2001).
[15] T. V. Pyrkov, I. S. Sokolov, and P. O. Fedichev, Aging (Albany NY) **13**, 7900 (2021).
[16] J. R. Poganik, B. Zhang, G. S. Baht, A. Tyshkovskiy, A. Deik, C. Kerepesi, S. H. Yim, A. T. Lu, A. Haghani, T. Gong, A. M. Hedman, E. Andolf, G. Pershagen, C. Almqvist, C. B. Clish, S. Horvath, J. P. White, and V. N. Gladyshev, Cell Metabolism **35**, 807 (2023).

F. Appendix C: Simulation of survival curves and finite-cohort inference

a. Model overview. Survival curves were generated from a coarse-grained stochastic dynamical model in which organismal state is described by a single slow variable $z(t)$ evolving near a fold (saddle-node) bifurcation. The dynamics follow an overdamped Langevin equation

$$\dot{z} = -\mu(t) + z^2 + \sqrt{2T_{\text{eff}}}\,\xi(t), \tag{14}$$

where $\mu(t)$ is a time-dependent stability parameter, T_{eff} is an effective noise amplitude, and $\xi(t)$ is Gaussian white noise with $\langle \xi(t)\xi(t')\rangle = \delta(t-t')$. The corresponding potential is $U(z,t) = \mu(t)z - z^3/3$, with a metastable minimum at $z_a = -\sqrt{\mu}$ and a barrier at $z_b = +\sqrt{\mu}$.

b. Aging dynamics. Aging is modeled as progressive loss of stability:

$$\mu(t) = \begin{cases} \mu_0, & t \le 20 \\ \mu_0 \left(1 - \frac{\gamma(t-20)}{100}\right)^2, & t > 20, \end{cases} \tag{15}$$

with $\mu_0 = 3.489$. The parameter γ controls the rate of damage accumulation and defines a collapse time $t_c = 20 + 100/\gamma$ at which $\mu(t) \to 0$.

c. Initial conditions. Initial states were drawn from the local equilibrium distribution near the stable minimum:

$$z(0) \sim \mathcal{N}\left(-\sqrt{\mu_0}, \sigma^2\right), \quad \sigma^2 = \frac{T_{\text{eff}}}{2\sqrt{\mu_0}}. \tag{16}$$

d. Metastable escape and terminal dynamics. Individuals were simulated using Euler–Maruyama integration with time step $dt = 0.01$ years. Entry into the unstable regime was defined by

$$z(t) > c\sqrt{\mu(t)}, \quad c = 2, \tag{17}$$

corresponding to crossing beyond the barrier into the nonlinear runaway regime.

Upon crossing, individuals transition to a terminal phase described by an unstable Ornstein–Uhlenbeck process, for which survival follows

$$S(t) = \operatorname{erf}\left(\frac{\gamma_u}{\sqrt{2}} e^{-\alpha t}\right), \tag{18}$$

with instability rate $\alpha = 0.5$ and scale parameter $\gamma_u = 0.7$. Remaining lifetimes were sampled by inverse transform sampling from the corresponding first-passage distribution.

e. Simulation details. Cohorts of $N = 4000$ individuals were simulated up to age 200 years. If individuals did not enter the unstable regime before t_c, transition was enforced at t_c. Survival curves were computed as

$$S(t) = \frac{1}{N} \sum_{i=1}^{N} \mathbb{I}(t_i > t), \tag{19}$$

where t_i denotes the simulated time of death.

f. Parameter sweeps. T_{eff} was varied over [2, 1.5, 1, 0.75, 0.5, 0.25, 0.1, 0.05, 0.025] at fixed $\gamma = 1$. Separately, γ was varied over [2.5, 2, 1.5, 1, 0.75, 0.5, 0.33] at fixed $T_{\text{eff}} = 1$.

g. Interpretation. Within this framework, T_{eff} modulates stochastic fluctuations and primarily affects early escape dynamics and mean lifespan, whereas γ governs the rate of stability loss and sets the overall lifespan scale, including maximum lifespan.

h. Finite-cohort sampling and apparent Gompertz behavior. To examine the effect of cohort size on inferred mortality dynamics, death times were also generated directly from the analytic survival function

$$S(t) = \operatorname{erf}\left(\frac{\gamma}{\sqrt{2}} e^{-\alpha t} \right), \tag{20}$$

which corresponds to the terminal unstable dynamics described above. This formulation produces an early low-mortality regime, an intermediate approximately exponential regime, and a late-life mortality plateau at $m(t) \to \alpha$.

Death times were sampled by inverse transform sampling:

$$t = \frac{1}{\alpha} \ln\left(\frac{\gamma}{\sqrt{2}\, \operatorname{erf}^{-1}(1-u)} \right), \qquad u \sim \mathcal{U}(0,1). \tag{21}$$

A large cohort ($n = 100{,}000$) was used to approximate the underlying hazard, and a smaller cohort ($n = 100$) was obtained by random subsampling without replacement.

i. Estimation of mortality. Deaths were binned into intervals of width $\Delta t = 1$ (corresponding to 12 hours), and time was reported in days. For each interval, the number of deaths d_t and individuals at risk N_t were computed, and the empirical mortality rate estimated as

$$\hat{m}(t) = \frac{d_t}{N_t \Delta t}. \tag{22}$$

In small cohorts, mortality estimates are quantized, with minimum nonzero value $1/N$. Intervals with zero deaths yield $\hat{m}(t) = 0$; for visualization on logarithmic axes, these were plotted at $0.5/N$, but this adjustment was not used in inference.

j. Gompertz inference. To assess whether finite cohorts yield apparent Gompertz behavior, mortality was modeled as

$$m(t) = Ae^{bt}. \tag{23}$$

Parameters were estimated using a binomial likelihood over all time intervals:

$$d_t \sim \text{Binomial}(N_t, p_t), \qquad p_t = 1 - e^{-m(t)\Delta t}. \tag{24}$$

This formulation incorporates zero-death intervals without pseudocounts and reflects the discrete sampling process. Parameters were obtained by maximum likelihood, and the mortality rate doubling time computed as

$$\text{MRDT} = \frac{\ln 2}{b}. \tag{25}$$

k. Parameterization. For the finite-cohort analysis, simulations were performed with $\alpha = 0.1$ and $\gamma = 6$. Under these conditions, the model predicts a mortality plateau at $m = \alpha$, an intermediate Gompertz-like regime with approximate doubling time $\ln(2)/\alpha$, and a median lifespan of order $1/\alpha$ (with a logarithmic correction set by γ).